PROCEEDINGS, Twenty-Seventh Workshop on Geothermal Reservoir Engineering
Stanford University, Stanford, California, January 28-30, 2002
SGP-TR-171

SALT LOADED HEAT PIPES: STEADY-STATE OPERATION AND RELATED HEAT AND MASS TRANSPORT

A. Simakin A. and A. Ghassemi

Department of Geology and Geological Engineering
University of North Dakota
Grand Forks, ND 58202
e-mail: ahmad_Ghassemi@mail.unda.nodak.edu

ABSTRACT

There is evidence suggesting that fluids in the root zone of many hydrothermal systems (at the brittle-ductile transition zone, about 3-4 km) can be highly saline. Therefore, fluid (state) can be expected to be in subcritical conditions and intensive multi-phase convection may occur at those depths. The particular type of fluid-solid interaction and as well as the fluid state depends on the fluid and rock compositions. This can be rather complicated involving several liquid and gaseous phases. As the simplest illustrative example, we consider the NaCl-H_2O system assuming the rock matrix to be chemically inert. When limited to three phases (NaCl-L-V), the critical curves and the pressures of the liquid-gas equilibrium in the system seem to be too low when compared with expected parameters of the root zone of the geothermal systems (T=380-450^{o}C). The fluid pressure is not well constrained and can be lower than hydrostatic due to active deformations that can increase rock porosity (fracture).

In this work we examine the model for a one-dimensional steady-state, two-phase gravity flow. The work involves derivation of the steady–state solution for mass balance equations for all components and fluid flow equations for the gas and liquid phases. Results show that in a three phase set (salt-water-gas), the plot of the steady-state liquid volume fraction, ε, vs. liquid temperature in the convecting column bifurcates into two sets of closed curves. Separation occurs because the maximum of the $P_{3b}(T)$ curve divides the entire P-ε plane into domains of solution-like and hydrous NaCl melt liquid phases. For the salt-unsaturated two-phase equilibrium, dependence of the steady-state liquid volume fraction describes a folded surface in the P-T-ε space. An estimate of the upper level of heat flux that can be transported through the salt loaded heat pipe yields a maximum of 10-15 W/m^2 at a permeability coefficient value, k, of about 10^{-15} m^2. Due to difference in the solubility of salt (or silicate materials) in the liquid and gas phases, heat transfer in salt loaded heat pipes is intrinsically connected to mass transfer. We suggest that the multi-phase convection of aggressive brines at high P-T can cause deep karst in the zone of dissolution. This process can be facilitated by hydrolysis with the acid that separates as a gaseous phase upon boiling. Assuming a solubility level of about 10 wt % and a permeability of 10^{-15} m^2 yields a net dissolution rate of 2-3 cm/yr. This is close to the subsidence rates measured in some geothermal fields. Mechanical deformation in the system may also play an important role in developing fluid pathways through continuously sealed areas separating geothermal fluid reservoirs in the brittle and ductile zones.

INTRODUCTION

Porous convection of the liquid and gaseous water mixture in hydrothermal systems can operate in the form of one-dimensional phase settling flow [Hardee, 1982]. Liquid in equilibrium with the gas phase has a higher density and permanently moves downward while gas rises. Gas-liquid equilibrium in the one-component system is monovariant and remains on the T(P) boiling curve that terminates at the critical point at T=374.0°C and P=220.6 bar. A column of the convecting liquid-gas mixture is bounded by two-phase transition Stefan fronts. Gas condenses at the upper surface while liquid boils upon reaching bottom. Essentially the maximum level of the heat flux that can be supported is defined by permeability and density contrasts. Mixture density distribution in the column can be gravitationally stable. This phenomenon is well studied and the influence of capillarity effects has been elaborated [McGuinness, 1996]. Such flows are called “heat pipes” and can transfer heat in excess of that by conduction alone [Hardee, 1982]. It is worth noting that the effectiveness of such flows (e.g., ratio of convective and conductive heat fluxes at given boundary temperatures) is higher than that of convection without phase transitions. Heat pipes heat transfer efficiency is connected to the high relative phase density differences and large heat of vaporization released at phase transition during flow in column.

Salted waters and brines are common fluids at the larger depth that are anticipated in hydrothermal systems. Another important feature of the heat pipe is the uniformity of heat flux in space. This is in contrast to the ordinary thermally driven porous media convection where the occurrence of rising and sinking limbs causes the surface heat flux to become spotty.

Deep geothermal wells drilled in active volcanic areas such as Nisyros (Chiodini et al. 1993b) and Mofete (Guglielminetti, 1986) have encountered brines. In colder geothermal systems, the brine layer is anticipated at a depth corresponding to the brittle-ductile transition depth (Lippmann et al. 1997). For example, in the Coso area relatively high salinity (3000 ppm of Cl) waters with temperature of 190^{o} C was found a 1477m deep hole (Duffield et al., 1980). It is likely that the contrast reflector reported by (Unruh and Monastero, 2001) near the brittle-ductile transition zone corresponds to the presence of a brine layer as anticipated for the Cerro Prieto geothermal field by Lippmann et al. 1997. The high temperature root of the hydrothermal zones are of commercial interest. Italy and Japan (Kasai et al., 2000; Barelli et al., 2000) have begun to exploit lower horizons of the traditional geothermal fields. In both cases acid brines had been encountered. One possible mechanism for brine generation is the separation of the rising magmatic fluid (crossing the critical point by decreasing pressure and temperature) into a gas-like and a liquid-like component (Giggenbach, 1987; Fournier, 1999). Salt concentrates in a dense liquid that can accumulate during active magma degassing at the brittle-ductile transition.

The goal of this work is to illuminate the main features and conditions for heat pipe convection of natural brines in hydrothermal systems. We consider some PT conditions that engender this process while considering the steady-state solution for the settling phase flow in a three-phase (salt-liquid-vapor) system and investigate the feature of possible solutions in the two-phase case.

BASIC CONCEPTS

One-dimensional convection due to phase settling in a column of porous rock is possible only in the presence of two phases (liquid-like and gas-like). For pure water, liquid and gas can coexist on the boiling curve below the critical conditions (P=220.6 bar and T=374.0°C). For water with dissolved salts, however, the two-phase equilibrium is bi-variant and occupies the area between two mono-variant curves (see Figure 1). One curve delineates the PT conditions for boiling in the presence of a salt and the second defines the critical curve of the two-phase equilibrium at a given temperature. Parameters of the critical curve depend on the salt composition with a shift to higher pressures for low NaCl (KCl)-$MgCl_2$-$CaCl_2$ (Tkachenko and Shmulovich 1992), as can be seen on the Figure 1.

Assuming that the lithostatic pressure is above 1 kbar, at a depth of 3-4 km brines will be in the liquid state precluding hetero-phase convection in any form. Generally, in tectonically stable conditions pressure switches from the hydrostatic regime to lithostatic at a depth of 3-4 km (P_s=1.0-1.5 kbar) (Connolly and Podladchikov, 2000). However, in some cases lower hydrostatic pressures can persist to a larger depth (e.g., as pointed out by Huenges et al., 1997, KTB drill hole revealed a hydrostatic pore fluid pressure to 9 km depth and T=265^{o}C). In the case of geothermal fields with high temperature gradient, the depth of the brittle-ductile rheological transition can be close to the depth of the hydrostatic – lithostatic pressure conversion.

Figure 1. *Generalized representation of the*

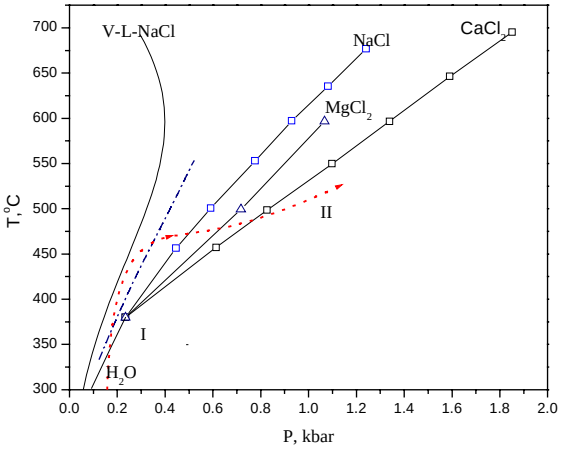

thermodynamic diagram of the water-salt system (based on the experimental data by Tanger and Pitzer, 1989; Tkachenko and Shmulovich, 1992).

The dotted arrow in Figure 1 shows a possible PT path for the geothermal root zone. This path can intersect the three-phase curve and the critical curve of the fluid with some dissolved salt at a higher PT i.e., larger depths (for a solute that is less soluble than NaCl the three phase curve is displayed using the dotted-dashed line). Effective convection involving phase separation and settling is possible in the PT interval between those two intersections. In the following a mathematical model is presented that describes convection with mass transfer of the dissolved substances. The mode is used to obtain estimates of the resulting steady state heat and mass fluxes.

MODEL EQUATIONS

Assuming that each phase obeys Darcy's law, flow in the two-component, two-phase system can be described by the following system of equations:

$$q_i = \frac{kk_{ri}(\varepsilon)}{\mu_i}\rho_i\left(\frac{\partial P}{\partial z} + \rho_i g\right): \quad (1)$$

where k_i ρ_l, P, q_i , μ_i, represent the permeability, density, pressure, volume flux, and the viscosity of the i^{th} phase, respectively; and ε is volume fraction of liquid in a two-phase fluid mixture. As for the one component water-vapor convective system, we assume the heat balance equation in terms of enthalpy to be valid:

$$\frac{\partial}{\partial t}(H_l\rho_l\varepsilon + H_g\rho_g(1-\varepsilon)) + \frac{\partial}{\partial z}\left(q_l H_l + q_g H_g\right) = \frac{\partial}{\partial z}\lambda\left(\frac{\partial}{\partial z}T\right): \quad (2)$$

where H_l and H_g are enthalpies of the liquid and gas phases. Additional equations describe the conservation of the solute in a liquid phase and in a gas phase, respectively:

$$\frac{\partial}{\partial t}(\phi\varepsilon\rho_l C_l) + \frac{\partial}{\partial z}(q_l C_l) = \Gamma_0 + \Gamma_1: \quad (3)$$

$$\frac{\partial}{\partial t}(\phi(1-\varepsilon)\rho_g C_g) + \frac{\partial}{\partial z}(q_g C_g) = -\Gamma_1 \quad (4)$$

Furthermore, we have the conservation of water in liquid phase and in as gas phase:

$$\frac{\partial}{\partial t}(\phi\varepsilon\rho_l (1-C_l)) + \frac{\partial}{\partial z}(q_l(1-C_l)) = \Gamma_2 \quad (5)$$

$$\frac{\partial}{\partial t}(\phi(1-\varepsilon)\rho_g (1-C_g)) + \frac{\partial}{\partial z}(q_g(1-C_g)) = -\Gamma_2 \quad (6)$$

where Γ_1 is a source function denoting the solute redistribution, Γ_2 is a source function accounting for boiling, Γ_O – is source function that describes dissolution and precipitation of the salt, ε represents the volume fraction of the liquid phase, ϕ is porosity, C is concentration of solute in gas (index g) and liquid (l), and ρ_1 and ρ_2 denotes the liquid density and gas density, respectively. Porosity will change due to dissolution of the solid phase. In the considered example, salt represents the solid phase while in reality solubility of silicate material in alkali saline solution should be considered:

$$\frac{d\varphi}{dt} = \frac{\Gamma_0(z)}{\rho_s} \quad (7)$$

Coupling with mechanical processes inducing matrix deformation can be achieved by including of the volumetric strain, liquid-gas pressure and solid phase source function into equations of the poroelasticity that are not presented here for simplicity. Three additional equations express the equilibrium of solute distribution, equilibrium of water in both phases, and equilibrium of solid salt with slat dissolved in liquid

$$\mu_{salt}(C_l, P, T) = \mu_{salt}(C_g, P, T) \quad (8)$$

$$\mu_{water}(C_l, P, T) = \mu_{water}(C_g, P, T) \quad (9)$$

$$\mu^s_{salt}(P, T) = \mu_{salt}(C_l, P, T) \quad (10)$$

The system with 11 unknowns (Γ_0, Γ_1, Γ_2, T, P, ε, q_l, q_g, C_l, C_g) is closed consisting of 11 equations 1-10. The steady state version of the model equation set is considered here as a first step. In doing so it is assumed that porosity is a slow variable and other variables can adjust to the rate of its variations. Furthermore, although permeability is a function of porosity, it is taken as a constant for the period considered. Indeed mechanical coupling (neglected here) can lead to the volumetric compaction that will compensate increases due to dissolution porosity.

Boundary conditions should not be specified for all variables. In the presence of excess salt three equations 8-9 express implicitly values of C_g, C_l, P as a functions of temperature. Temperature should have two boundary conditions such as heat flux and temperature on the lower boiling front. Source functions also have no boundary conditions and can be excluded from consideration. Fluxes q_l, q_g are linearly related and one constant defines net water flux through boiling front from the lower level. We consider a closed system here and some water enters from below only to compensate salt precipitation. In the steady state version volume fraction of liquid enters only into algebraic relation for the relative permeability and needs not boundary conditions.

MONO-VARIANT STATIONARY SOLUTION

In the case of three-phase equilibrium (S-L-V) boiling occurs at the fixed T at given P as in pure water. Difference consists in the nonzero sum of the liquid and gas fluxes due to the possible salt dissolution and deposition. At steady-state, the sum of the equations 3-6 is :

$$\frac{\partial}{\partial z}(q_l + q_g) = \Gamma_0(z) \quad (11)$$

By summation of the balance equations for water it is easy to get the relation between local gas and liquid fluxes for a closed system:

$$q_g = -q_l\frac{1-C_l}{1-C_g} \quad (12)$$

This defines a source function for solid connected with porosity change in the absence of mechanical deformation:

$$\frac{d\varphi}{dt} = \frac{\Gamma_0(z)}{\rho_s} = \frac{\partial}{\partial z}\left(\frac{q_l}{\rho_s}\frac{C_l - C_g}{1-C_g}\right) \quad (13)$$

However, since salt density is high and solubility is relatively small at the parameters considered (this approach can be even more valid for silicate –salt – water system to be considered) we neglect this effect for simplicity and assume that in steady state:

$$q_l + q_g = 0 \quad (15)$$

Using assumption the function $q_l(z)$ is obtained and can be inserted in (13) to get the first approximation for the dissolution function. By neglecting the difference in the phase enthalpies (related to different

heat capacities) in comparison with heat of evaporation, the heat balance equation is reduced to a rather simple form:

$$\frac{\partial}{\partial z}\left(q_l H_l + q_g (H_l + \Delta H_{vp})\right) = \frac{\partial}{\partial z}\lambda\left(\frac{\partial}{\partial z}T\right) \quad (16)$$

Or using (11) and integrating once:

$$-q_l \Delta H_{vp} + A = \lambda\left(\frac{\partial}{\partial z}T\right), \quad (17)$$

where the integration constant A is defined by boundary condition on the lower boundary and equal to the net heat flux from below (since $A = -q_l \Delta H_{vp} - \lambda\, \partial T / \partial z$) . The set of equations (8-10) for three-phase equilibrium is decoupled and defines boiling pressure P(T), phase compositions (C_l(T) and C_g(T)) and densities (ρ_l(T) and ρ_g(T))as the functions of temperature [Bischoff, 1991]. To complete formulation of the problem relative permeabilities should be specified. Relative permeability can be approximated as proportional to the volume fraction of the each phase:

$k_l^r = \varepsilon, \quad k_g^r = 1 - \varepsilon$

Tuncay and Ortoleva, 2001 used a model that connects relative permeability with the volume fraction of each phase ε_i^o when it becomes immobile, $\varepsilon_i > \varepsilon_i^o$ for flow.:

$k_l^r = (\varepsilon - \varepsilon_l^0)^n, \quad k_g^r = (1 - \varepsilon - \varepsilon_g^0)^n$

For the simplest case of relative permeability proportional to phase volume content system of equations (1,3) can be explicitly resolved to define pressure gradient and phase fluxes as:

$$\frac{\partial P}{\partial z} = -\frac{g(\varepsilon\rho_l^2\mu_g + \rho_g^2\mu_l(1-\varepsilon))}{\varepsilon\rho_l\mu_g + \rho_g\mu_l(1-\varepsilon)} \quad (18)$$

$$q_l = -kg\left(\frac{(\rho_l - \rho_g)\rho_g\rho_l\varepsilon(1-\varepsilon)}{\rho_l\mu_g\varepsilon + \rho_g\mu_l(1-\varepsilon)}\right) \quad (19)$$

Equations (18)-(19) can be expressed in non-dimensional by introducing natural scales for pressure P_o, for temperature equal to the character temperature difference ΔT_o, for density ρ_o, for viscosity μ_o, for length $L_o = P_o/\rho_o g$, for the mass flux $Q_o = kg\rho_o^2/\mu_o$. In the heat balance equation the only parameter of the problem arises

$$\gamma = \frac{\Delta H_{vp}\rho_o}{\Delta T_o c_{ps}\rho_s}\frac{q_o}{k_T/L_o} = Ste\frac{q_o}{k_T/L_o} \quad (20)$$

Parameter γ reflects efficiency of convective heat transfer relative conductive, constant A becomes heat flux in the units of the standard conductive heat flux $\lambda\Delta T_o/L_o$. Equations (17)-(19) will get the form (for the sake of clarity, normalized parameters designated as original ones)

$$\frac{\partial}{\partial z}T = -q_l\gamma + A \quad (21)$$

$$\Phi_1(\varepsilon, T) = \frac{\partial P}{\partial z} = -\frac{(\varepsilon\rho_l^2\mu_g + \rho_g^2\mu_l(1-\varepsilon))}{\varepsilon\rho_l\mu_g + \rho_g\mu_l(1-\varepsilon)} \quad (22)$$

$$\Phi_2(\varepsilon, T) = q_l = -\left(\frac{(\rho_l - \rho_g)\rho_g\rho_l\varepsilon(1-\varepsilon)}{\rho_l\mu_g\varepsilon + \rho_g\mu_l(1-\varepsilon)}\right) \quad (23)$$

Three-phase equilibrium in a two-phase system is mono-variant and space derivative of pressure can be expressed as

$$\frac{\partial P}{\partial z} = \frac{\partial P}{\partial T}\frac{\partial T}{\partial z} = \alpha(T)\frac{\partial T}{\partial z} \quad (24)$$

Therefore, equations (13-16) yield the implicit equation:

$$\Phi_1(\varepsilon, T) = \alpha(T)(\gamma\Phi_2(\varepsilon, T) + A) \quad (25)$$

It can be resolved numerically for the volume fraction of liquid as function of pressure with roots in the interval (0,1). Then using ε(T) and the relationship between P(z), T(z), ε(z), the distributions can be easily calculated. In Figure 3, the results of steady-state ε(T) projections are presented for different heat fluxes at the boiling front level. Values of A are expressed in the units of conductive heat flux $\lambda\Delta T/L_o$.). Common ε(T) curve has a closed structure due to convergence of densities at near-critical PT parameters and lowering of the convection efficiency. In the three-phase case, the curve is separated into two segments at the maximum vapor-pressure temperature. Multiply gas and liquid dominated solutions converge to the single solution with ε_l=0.5, ε_g=0.5 as the value of T approaches T_{max}, the temperature corresponding to the maximum pressure of the three-phase equilibrium from below. While in the more concentrated and higher temperature part (NaCl melts in extreme conditions) there are two asymptotic solutions with ε_l=1, ε_g=1 as T approaches T_{max}. The explicit relations (18) and (19) cannot be solved analytically when using more complex expressions for relative permeability, and the system of equations (1, 15, 17) will need to be solved numerically. Results of calculations with relative phase permeabilities that are proportional to the second order polynomials of their volume Fractions are demonstrated in Figure 3.

Figure 3. *An example of the steady-sate distribution of the liquid phase fraction in the heat pipe operating in the system NaCl-H2O as a function of temperature.*

They emphasize that due to the larger inter-phase density differences convection in the salty part is more intensive. For example at non-dimensional heat flux A=60 convection is active in concentrated domain but wanes in the diluted domain. To express the maximum heat flux in dimensional form, we use a scale coefficient 0.29 W/m^2 obtained at k = $3\cdot10^{-16}$ m^2, constant viscosities for the liquid ($2.93\text{x}10^{-3}$ poise) and for the gas phase ($1.2\text{x}10^{-4}$ poise), and a thermal conductivity coefficient κ_T of 0.01 cm^2/s. Other parameters correspond to the thermodynamic properties of phases. Then, the maximum heat flux will be around 15-18 W/m^2. In effect, the distribution of the approximate volumetric dissolution rate (initially neglected) in a column can be found by integrating Eqn.13 with known T(z) inserted into relations for q_l, C_l and C_g.

CONVECTION IN TWO-PHASE SYSTEM

Three-phase equilibrium in NaCl-H2O system can be expected at rather exotic conditions– low pressure and high temperature (like sill intrusions or shallow volcanic magma chamber). The two-phase PT domain is extended to higher than three-phase pressures. But in the two-phase case, at least one end of the column is not bounded by a three-phase front with excess salt that can compensate, by dissolution–precipitation, for any difference in the vapor and liquid composition. We suggest that this can be achieved while including diffusion mass transport into the equation or by a more detailed description of the mixing process at the single droplet level. Despite the true structure of the boundary layers inside the column, processes of the salt exchange between the phases, fluid segregation (or formation of more concentrated fluid by volumetric boiling of the descending liquid in the thermal gradient) or mixing can occur in accordance with equations (3)-(6) by means of nonzero source terms involved.

In two-phase area pressure and temperature can vary between critical and the three-phase curve therefore, the solution of the steady-state analogue of Eqn. (25) would be a surface in (ε,P,T) space. We can define $q_l(z)$ by summing equations (3) and (4):

$$\frac{\partial}{\partial z}(q_l(C_l - C_g) = 0 \text{ or } q_l(C_l - C_g) = B, \qquad (26)$$

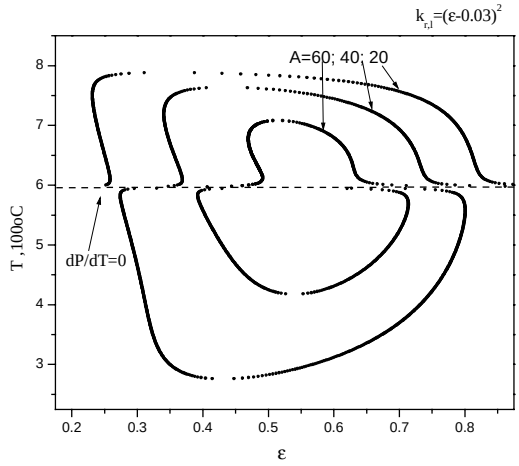

where the constant B is to be found from boundary conditions. Its value corresponds to heat flux at the boiling boundary. From (26) and (19) it follows that for a linear k_r:

$$\frac{B}{C_l - C_g} = -kg\frac{(\rho_l - \rho_g)\rho_g\rho_l\varepsilon}{\rho_l\mu_g\varepsilon/(1-\varepsilon) + \rho_g\mu_l}, \qquad (27)$$

where at a given T, pressure P⊂ ($P_{S\text{-}L\text{-}V}(T)$, $P_{crit}(T)$). After approximating the functions $C_l(P,T)$, $C_g(P,T)$, $\rho_l(P,T)$, $\rho_g(P,T)$ for two-phase zone, one can easily define the $\varepsilon_{st}(P,T)$ function. Then, by integrating equations (17,18) the distributions P(z) and T(z) can be obtained.

Equation (27) is non-dimensionalized by introducing a scale for the porous flow mass flux as $Q_o = kg\rho_o^2/\mu_o$. Another simplification consists of the assumption that viscosities of the liquid and fluid phase are proportional to their densities $\mu = \overline{\mu}\rho_i$. After taking $\mu_o = \overline{\mu} = \mu_{ol}$, Equation (27) will have a very simple form:

$$\frac{B}{(C_l - C_g)(\rho_l - \rho_g)} = \varepsilon(1-\varepsilon), \qquad (28)$$

where B is expressed in units of Q_o. The solution has two branches and they are the two roots of square polynomial (28):

$$\varepsilon_1 = \frac{1+\sqrt{1-4B^*}}{2}, \varepsilon_2 = \frac{1-\sqrt{1-4B^*}}{2} \qquad (29)$$

where the parameter B*(P,T) is equal to the left side of Equation (28). The first root corresponds to the higher liquid fractions or liquid–dominated solution, while the second root stands for the gas–dominated fraction.

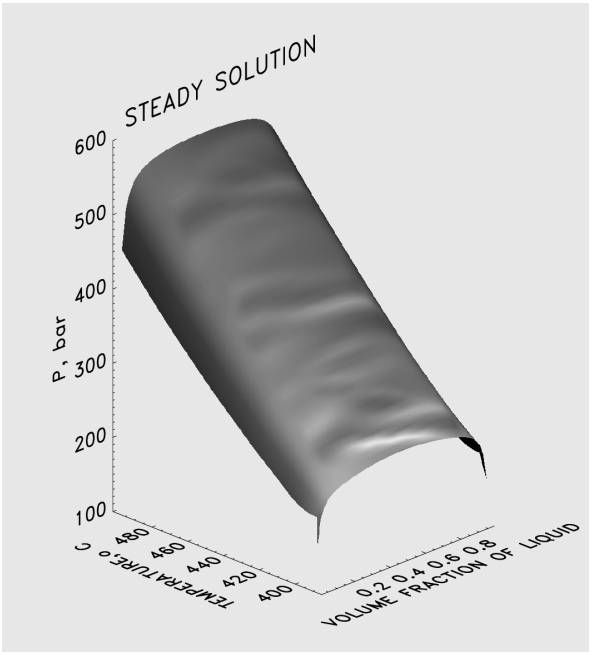

Figure 4. *3D plot of the steady-state liquid fraction distribution in a heat pipe operating in L-V part of the equilibrium NaCl-H2O system. Two values of the water mass flux are used in non-dimensional form (B=0.01 see eqn.26). Surfaces ε(P,T) are cut by vertical surface P(T) of three phase equilibrium*

To complete the solution we use experimental data on the composition and densities of the co-existing liquid-gas phases in the NaCl-H_2O system in the temperature range of 380 and 500°C that corresponds to a pressure range of 200-600 bar. The lowest pressure in each section corresponds to the three-phase equilibrium (salt-vapor-water) and the highest to the critical pressure. Individual isothermal sections of $C_l(P)$ –$C_g(P)$ and $\rho_l(P)$-$\rho_g(P)$ have been approximated with polynomials of up to 8th order with accuracy close to experimental error. Sufficiently smooth interpolations are performed between sections using the pressures in adjacent sections and normalizing them by their maximum values. Configuration of the distribution of the steady-state liquid fraction, ε, in the ε-P-T space is calculated using Eqn. 29 and experimental data for phase densities and compositions at B=0.01 and displayed in Figure 4.

It is obvious that solution exists only for a limited range of the mass and corresponding heat fluxes. At sufficiently high values of liquid flux (B*=1/4) the expression under a radical becomes zero. Hydrothermal system of the type described can provide heat fluxes lower than this critical level. One can estimate this threshold level as (one multiplier equals ρo is used to transform ρ_l -ρ_g into dimensional form):

$$Q_{crit} = \frac{B_{crit}}{(C_l - C_g)} = \frac{kg\rho_o(\rho_l - \rho_g)}{4\overline{\mu}} \qquad (30)$$

Associated critical convective heat flux is $\Delta H_{vp} Q_{crit}$, where ΔH_{vp} is a heat of vaporization.

For the pure thermal convection in the porous media approximate formula is valid that determines heat transport across fluid saturated layer with temperature difference ΔT (e.g. Trubitsyn et al., 1993):

$$Q = 0.218\,\Delta H\sqrt{U_T U_f},\ U_T = \frac{\kappa_T}{L},\ U_f = \frac{kg\Delta\rho(\Delta T)}{\mu}$$

and characteristic enthalpy increment equals to $\Delta H=\rho_s c_{ps}\Delta T$ and density difference is proportional to temperature difference $\Delta\rho=\alpha\Delta T$, α is thermal expansion coefficient. Or heat flux is medium geometric between conductive and convective with neglected diffusion. Rate scale associated with thermal conduction decreases with vertical extension of convecting domain L. It should be noted that enthalpy of vaporization (2000 J/g) is higher than characteristic enthalpy difference ($\Delta T_o c_{ps}\rho_s$ =520 J/g at ΔT_o=200°C, ρ_{os}=2.6 g/cm^3, c_{ps}=1 J/g/o) connected with simple heating and density difference is higher too. Some particular values of parameters can be inserted for illustration:

For the heat pipe estimates typical value of density difference can be taken as (for the far from critical conditions) $\Delta\rho$=0.8g/cm^3, ρo is to be set 1g/cm3, viscosity is assumed to be $3\cdot10^{-3}$ poise. Enthalpy of the vaporization is about 2000 J/g. Value of the permeability is the least constrained. Its value depends on the porosity and fracture density and pattern and can vary in orders 10^{-15}-10^{-18}m^2. At permeability 10-15m^2 maximum associated heat flux will be about 13 W/m^2 or for the location 3x3 km about 120 MW. The lowest permeability will make contribution of this convection to the heat balance negligible (0.12 MW). At the same time heat transfer rate through the thermally convecting fluid with parameters: ΔTo=200°C, $\rho_{o,s}$=2.6 g/cm3, $c_{p,s}$=1 J/g/o, L=500 m, $k_T=10^{-2}$ cm^2/s, $\alpha=3\cdot10^{-3}$, $k=10^{-15}$ m^2 - will be 0.9 W/m^2.

ESTIMATES OF THE MASS FLUX AND DISSOLUTION RATE

Any thermal flow in a porous matrix will cause dissolution–precipitation of solid minerals composing rock and porosity change due to temperature dependence of the solubility. The rate of these processes depends on the convection rate and solubility changes on the flow path. Brines at the parameters of brittle-ductile transition are rather aggressive and can cause intensive corrosion of surrounding rocks. Based on equilibrium thermodynamics Durst and Vuataz, 2001 estimated that injection of NaCl brine into a well at relatively

low PT parameters (P= 40 MPa, T=165°C, porosity 10%) will double porosity of carbonate containing matrix. It is important to note that phase separation leads to the formation of the reactive fluids from the neutral ones due to hydrolysis (especially of earth-alkaline salts as $CaCl_2$) and portioning of the acid components into vapor and alkaline (NaOH, $Ca(OH)_2$) into liquid (Fournier, 1999).

For the heat pipe operating on the pure water in silicate matrix effects of the solid matrix solubility can be neglected and it will transfer only heat. However, assuming that salted water or brine is involved mass flux will be combined with heat transfer. In the model considered interaction of the brine with silicate matrix is not considered. Therefore chemical flux is considered in the terms of the dissolved salt. On the boiling front precipitation rate is easily recovered that equals difference of the incoming with liquid salt and leaving with vapor:

$$\frac{dM}{dt}/S = q_s = q_l(C_l - C_g)\Big|_{T(z)=Tb} \qquad (31)$$

Indeed at steady state operation of the system this salt should be gained at the condensation front and partially collected by the way to boiling front due to effective dissolution of salt (in our approximation). In the solution for three-phase (HLV) case we neglect this effect and get simplified relationship $q_l=-q_g$. But there is also volumetric dissolution rate term Γo defined by Eqns. 11,12. In the considered model main dissolution-precipitation events have place on the ends of pipe, but at more detailed consideration of the water-salt-silicate system it will be distributed in the whole flow path. Nevertheless net dissolution rate will be defined by Eqn. 31. Maximum dissolution rate of surrounding rocks can be estimated in the same way as maximum convective heat flux rate (see Eq. 30) by setting solubility of silicate material in a hot alkaline brine as $C_l=0.1$ and $C_g=0$. The upper estimate of the linear effective dissolution rate (q_s/ρ_s) will be 1-2 cm/yr. It corresponds to the assumed permeability of 10^{-15} m^2.

DISCUSSION

The phase convection considered in this study engenders a continuous mass transfer mechanism that can be a cause of the surface subsidence observed in some active geothermal fields. For example, field observations in the Geysers geothermal system for the last 20 years demonstrate a maximum subsidence rate of 4.5±0.5 cm/yr. In practice, this is equivalent to the value of 5 cm/yr that was measured before exploitation (1973-1977) (Mossop et al., 1997). The subsidence rate is practically constant and does not depend on the local effect of heat production. Also, in the Coso case, subsidence figures are similar, i.e., a global subsidence rate of 3.5 cm/yr (Wicks et al., 2001). The location of the source responsible for the surface distribution of the subsidence rate corresponds to a depth of 4.6-3.9 km for Coso geothermal field (Wicks et al., 2001) and 4.1-3.8 km for the Geysers. Both determinations fit the position of the upper part of the brittle-ductile transition zone. When interpreting the surface subsidence, Wicks et al. 2001 found that the pressure drop in the layer at 1.5-0.4 km should be as large as 10-100 MPa. This suggests that the mean stress in the solid matrix should be lower (on the order of 0.1-1 kbar). For an abnormal thermal gradient, this pressure may correspond to a depth equal to that of the rheological brittle-ductile where pore pressure can be very low too. Unruh and Monastero (2001) have confirmed the rheological transition (brittle to ductile) in Coso geothermal field. According to their study, seismic imaging indicates that the Quaternary –active Coso Hot Spring fault appears to flatten downward and may merge with a reflective horizon at a depth of 4 km. This is interpreted as the brittle-ductile transition zone. It is suggested that a high amplitude reflector found at a depth of 6 km beneath the geothermal field that can be a lens of fluid rather than a sill.

Our estimates of the underground volumetric karst rate, expressed as the velocity of the linear dissolution, have an order of magnitude that is similar to the field measurements of the subsidence rate. Whether fluid is hetero-phase at depth or not mainly depends on the pressure and composition of the dissolved matter. Our scheme of the two-phase convection summarized in Figure 5 is particularly relevant when a real fluid composition including both salts and possibly silica is considered. Active tectonic processes that produce additional pore (crack) space as well as the dissolution process itself can reduce the fluid pressure to the levels of phase separation.

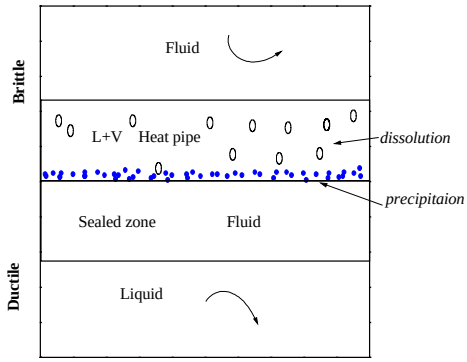

Figure 5. *Sketch of the possible distribution of the saline fluid state and circulation pattern in the root zone of a geothermal system on the level of the brittle-ductile transition.*

It should be emphasized that according to our model, the dissolution process may operate continuously. This is in contrast to the periodic pressurization with increase in the porosity of the lower brittle aquifers (Wicks et al. 2001). In the latter case, an exponential surface level decrease similar to that observed by

Gaeta et al., 1998 is to be expected. Additional theoretical modeling of the combined convective, chemical, and mechanical processes as well as geophysical observations are necessary to clarify the actual mechanism of heat and mass transfer in the root zone of geothermal systems having no links to modern magmatism.

REFERENCES

Barelli, A., Bertini, G., Buonasorte, G., Cappetti, G. and Fiordelisi, A., 2000. Recent deep exploration results at the margins of the Larderello-Travale geothermal system. Proceedings of the World Geothermal Congress 2000-Japan, 965-970.

Bischoff, J.L., 1991. Densities of liquids and vapors in boiling NaCl-H2O solutions: a PVTX summary from 300 to 500°C. *Amer. J. Sci.*, **291**, 309-338.

Chiodini, G., Marini, L., Russo, M., 2001. Geochemical evidence for the existence of high-temperature hydrothermal brines at Vesuvio volcano, Italy. *Geochim. Cosmochim. Acta*, **65**, 2129-2147.

Connolly, J.A.D. and Podladchikov, Yu.Yu., 2000. Temperature-dependent viscoelastic compaction and compartmentalization in sedimentary basins. *Tectonophysics*, **324**, 137-168.

Duffield, W., Bacon, C.R. and Dalrymple, G.B., 1980. Late Cenozoic Volcanism, Geochronology, and structure of Coso Range, Inyo County, California. *J Geophys. Res.*, **85**, N.B5, 2381-2404.

Durst, P., Vuataz, F.D., 2001. Geochemical modeling of the Soultz-sous-Forests Hot Dry system. Brine-Rock interactions in a deep hot fractured granite reservoir. Proc., 26th Workshop on Geothermal Reservoir Engineering, Stanford University, Stanford, California, January 29-31, 2001.

Fournier, R.O., 1999. Hydrothermal processes related to movement of fluid from plastic to brittle rocks in magmatic epithermal environment. *Econ. Geol*., **94**, 1193-1211.

Gaeta, F.S., DeNatale, G., Peluso, F., Mastrolorenzo, G., Castagnolo, D., Troise, C., Pingue, F., Mita, D.G. and Rossano, S., 1998. Genesis and evolution of unrest episodes at Campi Flegrei caldera – the role of thermal fluid-dynamical processes in the geothermal system. *J. Geophys. Res.*, **103**, N.9, 20921-20933.

Giggenbach, W. F., 1997. The origin and evolution of fluids in magmatic-hydrothermal systems. In H. L. Barnes (ed.) *Geochemistry of Hydrothermal Ore Deposits*, 3rd Edition, pp. 737–796, John Wiley & Sons, New York.

Guglielminetti, M., 1986. Mofete geothermal field. *Geothermics* **15**, 781–790.

McGuinness, M.J., 1996. Steady state soluiton selection and existence in geothermal heat pipes. I: the convective case. *Int. J. Heat and Mass Transfer*, **39**, No.2, 259-274.

Hardee, H.C., 1982. Permeable convection above magma bodies. *Tectonophysics*, **84**, 179-195.

Huenges, E. ; Erzinger, J., Kück, J., Engeser, B., Kessels, W., 1997. The permeable crust: Geohydraulic properties down to 9101 m depth *J. Geophys. Res.*, **102,** 18.255-18.265.

Kasai, K., Hishi Y., Fukuda, D., Kato, O., Doi, N., Akaku, K., Ominato, T. and Tosha, T. 2000. The fluid chemistry and reservoir model for the Kakkonda geothermal system, obtained by NEDO's deep seated geothermal reservoir survey, Japan. Proceedings of the World Geothermal Congress 2000-Japan, 1325-1330.

Lippmann, M.J., Truesdell, A.H. and Gutierrez, P. 1997. What will a 6 km deep well at Cerro Prieto find. Proc. 21th Workshop on Geothermal Reservoir Engineering. Stanford University, Stanford, California, Jan. 27-29, pp.19-28.

Mossop A.M., Murray D., Owen, S., and Segall, P., 1997. Subsidence at the geysers geothermal field: Results and simple models. Proc. 21th Workshop on Geothermal Reservoir Engineering. Stanford University, Stanford, California, Jan. 27-29, pp. 377-382.

Tanger, J.C. and Pitzer, K.S., 1989. Thermodynamics of NaCl-H2O: A new equation of state for near-critical region and comparisons with other equations for adjoining regions. *Geochim. et Cosmochim. Acta*, **53,** 973-987.

Tkachenko, S.I. and Shmulovich, K.I., 1992. Liquid-Vapor equilibrium at 400 to 600oC in aqueous system containing NaCl, KCl, CaCl2 and MgCl2. Translated from: *Dokladi Rossiyskoy Akademii Nauk*, **326**, No.6, pp. 1055-1059.

Tuncay, K. and Ortoleva, P., 2001. Salt tectonics as a self-organizing process: a three dimensional reaction, transport and mechanical model (preprint).

Unruh, J. and Monastero, F., 2001. New seismic imaging of the Coso geothermal field, Eastern California. Proc. 26th Workshop on Geothermal Reservoir Engineering, Stanford University, Stanford, California, Jan. 29-31.

Wicks, C., Thatcher, W., Monastero, F., and Hating, M., 2001. Steady-State Deformation on the Coso Range, East-Central California, Inferred from Satellite Radar Interferometry, *J. Geophys. Res.*(in press).